

PARALLEL PROJECTION MODELLING FOR LINEAR ARRAY SCANNER SCENES

M. Morgan^a, K. Kim^b, S. Jeong^b, A. Habib^a

^a Department of Geomatics Engineering, University of Calgary, Calgary, 2500 University Drive NW, Calgary, AB, T2N 1N4, Canada - (mfmorgan@ucalgary.ca, habib@geomatics.ucalgary.ca)

^b Electronics and Telecommunications Research Institute (ETRI), 161 Gajeong-Dong, Yuseong-Gu, Daejeon, 305-350, Korea – (kokim, soo)@etri.re.kr

PS WG III/1: Sensor Pose Estimation

KEY WORDS: Photogrammetry, Analysis, Modelling, Method, Pushbroom, Sensor, Stereoscopic, Value-added

ABSTRACT:

Digital frame cameras with resolution and ground coverage comparable to those associated with analogue aerial cameras are not yet available. Therefore, linear array scanners have been introduced on aerial and space borne platforms to overcome these drawbacks. Linear array scanner scenes are generated by stitching together successively captured one-dimensional images as the scanner moves. Rigorous modelling of these scenes is only possible if the internal and external characteristics of the imaging system (interior orientation parameters and exterior orientation parameters, respectively) are available. This is not usually the case (e.g., providers of IKONOS scenes do not furnish such information). Therefore, in order to obtain the parameters associated with the rigorous model, indirect estimation has to be performed. Space scenes with narrow angular field of view can lead to over-parameterization in indirect methods if the rigorous model is adopted. Earlier research has established that parallel projection can be used as an alternative/approximate model to express the imaging process of high altitude linear array scanners with narrow angular field of view. The parallel projection is attractive since it involves few parameters, which can be determined using limited number of ground control points. Moreover, the parallel projection model requires neither the interior nor the exterior orientation parameters of the imaging system. This paper outlines different parallel projection alternatives (linear and nonlinear). In addition, forward and backward transformations between these parameters are introduced. The paper also establishes the mathematical relationship between the navigation data, if available, and the parallel projection parameters. Finally, experimental results using synthetic data prove the suitability of parallel projection for modelling linear array scanners and verify the developed mathematical transformations.

1. INTRODUCTION

The limited number of pixels in 2-D digital images that are captured by digital frame cameras limits their use in large scale mapping applications. On the other hand, scenes captured from linear scanners (also called pushbroom scanners or line cameras) have been introduced for their great potential of generating ortho-photos and updating map databases (Wang, 1999). The linear scanners with up-to one-meter resolution from commercial satellites could bring more benefits and even a challenge to traditional topographic mapping with aerial images (Fritz, 1995).

Careful sensor modelling has to be adapted in order to achieve the highest potential accuracy. Rigorous modelling describes the scene formation as it actually happens, and it has been adopted in a variety of applications (Lee and Habib, 2002; Habib et al., 2001; Lee et al., 2000; Wang, 1999; Habib and Beshah, 1998; McGlone and Mikhail, 1981; Ethridge, 1977).

Alternatively, other approximate models exist such as rational function model, RFM, direct linear transformation, DLT, self-calibrating DLT and parallel projection (Fraser et al., 2001; Tao and Hu, 2001; Dowman and Dolloff, 2000; Ono et al., 1999; Wang, 1999; Abdel-Aziz and Karara, 1971). Selection of any approximate model, as an alternative, has to be done based on the analysis of the achieved accuracy. Among these models, parallel projection is selected for the analysis. The rationale and the pre-requisites behind its selection are discussed as well as its linear and non-linear mathematical forms are presented in

Section 3. But first, background information regarding linear array scanner scenes is presented in Section 2. In cases where scanner navigation data are available, Section 4 sets up their relationship to the parallel projection model. Due to the complexity of the derivation of the developed transformations, Section 5 aims at verifying them by using synthetic data. Finally, Section 6 includes the conclusions and recommendations for future work.

2. BACKGROUND

2.1 Motivations for using Linear Array Scanners

Two-dimensional digital cameras capture the data using a two-dimensional CCD array. However, the limited number of pixels in current digital imaging systems hinders their application towards extended large scale mapping functions in comparison with scanned analogue photographs. Increasing the principal distance of the 2-D digital cameras will increase the ground resolution, but will decrease the ground coverage. On the other hand, decreasing the principal distance will increase the ground coverage at the expense of ground resolution.

One-dimensional digital cameras (linear array scanners) can be used to obtain large ground coverage and maintain a ground resolution comparable with scanned analogue photographs. However, they capture only a one-dimensional image (narrow strip) per snap shot. Ground coverage is achieved by moving the scanner (airborne or space borne) and capturing more 1-D

images. The scene of an area of interest is obtained by stitching together the resulting 1-D images. It is important to note that every 1-D image is associated with one-exposure station. Therefore, each 1-D image will have different Exterior Orientation Parameters (EOP). A clear distinction is made between the two terms “scene” and “image” throughout the analysis of linear array scanners, Figure 1.

An **image** is defined as the recorded sensory data associated with one exposure station. In the case of a frame image, it contains only one exposure station, and consequently it is one complete image. In the case of a linear array scanner, there are many 1-D images, each associated with a different exposure station. The mathematical model that relates a point in the object space and its corresponding point in the image space is the collinearity equations, which uses EOP of the appropriate image (in which the point appears).

In contrast, a **scene** is the recorded sensory data associated with one (as in frame images) or more exposure stations (as in linear array scanners) that covers near continuous object space in a short single trip of the sensor. Therefore, in frame images, the image and scene are identical terms, while in linear array scanners, the scene is an array of consecutive 1-D images.

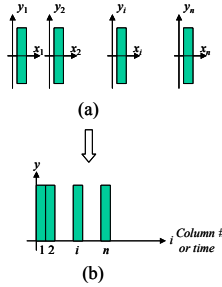


Figure 1. A sequence of 1-D images (a) constituting a scene (b)

2.2 Rigorous Modelling of Linear Array Scanners

Rigorous (exact) modelling of linear array scanners describes the actual geometric formation of the scenes at the time of photography. That involves the Interior Orientation Parameters (IOP) of the scanner and the EOP of each image in the scene. Representation of EOP, adopted by different researchers (Lee and Habib, 2002; Lee et al., 2000; Wang, 1999; McGlone and Mikhail, 198; Ethridge, 19771), includes:

- Polynomial functions - This is motivated by the fact that EOP do not abruptly change their values between consecutive images in the scene, especially for space-based scenes.
- Piecewise polynomial functions - This option is preferable if the scene time is large, and the variations of EOP do not comply with one set of polynomial functions.
- Orientation images – In this case, EOP of selected images (called orientation images) within the scene are explicitly dealt with. EOP of other images are functions of those of the closest orientation images. This option also avoids using one set of polynomial functions throughout the scene.
- Non-polynomial representation – This option explicitly deals with all the EOP associated with the involved scene. Linear feature constraints can be used to aid independent recovery of the EOP of the images

as well as to increase the geometric strength of the bundle adjustment.

EOP are either directly available from navigation units such as GPS/INS mounted on the platform, or indirectly estimated using ground control in bundle adjustment (Habib and Beshah, 1998; Habib et al., 2001; Lee and Habib, 2002). For indirect estimation of the polynomial coefficients using Ground Control Points (GCP), instability of the bundle adjustment exists, especially for space-based scenes (Wang, 1999; Fraser et al., 2001). This is attributed to the narrow Angular Field of View (AFOV) of space scenes, which results in very narrow bundles in the adjustment procedures. For this reason, a different model, parallel projection, will be sought for the analysis in Section 3.

3. PARALLEL PROJECTION

3.1 Motivations

The motivations for selecting the parallel projection model to approximate the rigorous model are summarized as follows:

- Many space scanners have narrow AFOV – e.g., it is less than 1° for IKONOS scenes. For narrow AFOV, the perspective light rays become closer to being parallel.
- Space scenes are acquired within short time – e.g., it is about one second for IKONOS scenes. Therefore, scanners can be assumed to have same attitude during scene capturing. As a result, the planes, containing the images and their perspective centres, are parallel to each other.
- For scenes captured in very short time, scanners can be assumed to move with constant velocity. In this case, the scanner travels equal distances in equal time intervals. As a result, same object distances are mapped into equal scene distances.

Therefore, many space scenes, such as IKONOS, can be assumed to comply with parallel projection.

3.2 Forms of Parallel Projection Model

Figure 2 depicts a scene captured according to parallel projection. Scene parallel projection parameters include: two components of the unit projection vector (L , M); orientation angles of the scene (ω , ϕ , κ); two shift values (Δx , Δy); and scale factor (s). Utilizing these parameters, the relationship between an object space point $P(X, Y, Z)$, and the corresponding scene point $p(x, y')$ can be expressed as:

$$\begin{bmatrix} x \\ y' \\ 0 \end{bmatrix} = s \cdot \lambda \cdot R^T \begin{bmatrix} L \\ M \\ N \end{bmatrix} + s \cdot R^T \begin{bmatrix} X \\ Y \\ Z \end{bmatrix} + \begin{bmatrix} \Delta x \\ \Delta y \\ 0 \end{bmatrix} \quad (1)$$

where:

R is the rotation matrix between the object and scene coordinate systems;

N is the Z-component of the unit projection vector - i.e., $N = \sqrt{1 - L^2 - M^2}$; and

λ is the distance between the object and image points, which can be computed from the third equation in (1).

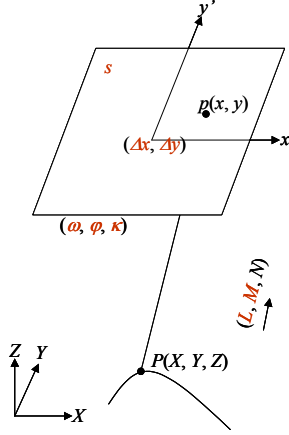


Figure 2. Parallel projection parameters

Equations 1 represent a non-linear form of the parallel projection model. They can be reduced to a linear form, Equations 2:

$$\begin{aligned} x &= A_1 X + A_2 Y + A_3 Z + A_4 \\ y' &= A_5 X + A_6 Y + A_7 Z + A_8 \end{aligned} \quad (2)$$

where A_1 to A_8 are the linear parallel projection parameters, and will be referred to as “2-D Affine parameters” (Ono et al., 1999). It is important to mention that Equations 1 are useful if scanner navigation data are available (the derivation of scene parallel projection parameters from the navigation data is presented in Section 4). On the other hand, if GCP are available, the linear model in Equations 2 becomes easier to use. The relationship between the linear and non-linear forms is summarized in the following subsection.

3.3 Transformation between Parallel Projection Forms

3.3.1 Transformation from the Non-Linear to the Linear Form
Knowing the scene parallel projection parameters, intermediate parameters (U , V) can be computed as expressed in Equations 3. Afterwards, the 2-D Affine parameters are computed.

$$\begin{aligned} U &= \frac{r_{11}L + r_{21}M + r_{31}N}{r_{13}L + r_{23}M + r_{33}N} \\ V &= \frac{r_{12}L + r_{22}M + r_{32}N}{r_{13}L + r_{23}M + r_{33}N} \\ A_1 &= s(r_{11} - r_{13}U) & A_5 &= s(r_{12} - r_{13}V) \\ A_2 &= s(r_{21} - r_{23}U) & A_6 &= s(r_{22} - r_{23}V) \\ A_3 &= s(r_{31} - r_{33}U) & A_7 &= s(r_{32} - r_{33}V) \\ A_4 &= \Delta x & A_8 &= \Delta y \end{aligned} \quad (3)$$

where r_{11} to r_{33} are the elements of the rotation matrix R . The derivation of this transformation can be found in (Morgan, 2004). Next subsection deals with the reverse of such transformation.

3.3.2 Transformation from the Linear to the Non-Linear Form
Knowing the 2-D Affine parameters, scene parallel projection parameters can be derived in three steps:

Step 1: Components of the projection vector have to be computed as expressed in Equations 4.

$$\begin{aligned} L' &= \frac{A_3}{\sqrt{\left(\frac{A_1 A_7 - A_3 A_5}{A_3 A_6 - A_2 A_7}\right)^2 (A_2^2 + A_3^2) + \left(\frac{A_1 A_7 - A_3 A_5}{A_3 A_6 - A_2 A_7}\right) 2 A_1 A_2 + A_1^2 + A_3^2}} \\ M' &= L' \frac{A_1 A_7 - A_3 A_5}{A_3 A_6 - A_2 A_7} \\ N' &= \frac{-L' A_1 - M' A_2}{A_3} \\ L &= L' \frac{N'}{|N'|} \\ M &= M' \frac{N'}{|N'|} \\ N &= |N'| \end{aligned} \quad (4)$$

Step 2: The scale factor can be computed as expressed in Equations 5, by first computing intermediate parameters (T_1 , T_2 , T_3 , A , B , C , U and V).

$$\begin{aligned} T_1 &= A_1^2 + A_2^2 + A_3^2 \\ T_2 &= A_5^2 + A_6^2 + A_7^2 \\ T_3 &= A_1 A_5 + A_2 A_6 + A_3 A_7 \\ A &= T_3^2 - T_1 T_2 \\ B &= 2 T_3^2 + T_1^2 - T_1 T_2 \\ C &= T_3^2 \\ U &= \sqrt{\frac{-B - \sqrt{B^2 - 4AC}}{2A}} \frac{L}{|L|} \\ V &= \frac{T_3 (1 + U^2)}{T_1 U} \\ s &= \sqrt{\frac{T_1}{1 + U^2}} \end{aligned} \quad (5)$$

Step 3: Finally, the scene orientation angles can be computed as expressed in Equations 6, by first computing intermediate parameters (D , E , and F).

$$\begin{aligned} D &= U^2 + V^2 + 1 \\ E &= 2U \frac{A_1}{s} + 2V \frac{A_5}{s} \\ F &= \frac{A_1^2}{s^2} + \frac{A_5^2}{s^2} - 1 \\ \varphi &= \arcsin \left(\frac{-E + \frac{L}{|L|} \sqrt{E^2 - 4DF}}{2D} \right) \\ \kappa &= \arctan \left(\frac{-V \sin \varphi + \frac{A_5}{s}}{\cos \varphi} \right) \\ &= \arctan \left(\frac{U \sin \varphi + \frac{A_1}{s}}{\cos \varphi} \right) \end{aligned}$$

$$\omega = \arcsin \left(\frac{\frac{A_2}{s} \sin \varphi \cos \kappa + \frac{A_2}{s} U \cos \varphi + \frac{A_3}{s} \sin \kappa}{\sin^2 \kappa + (\sin \varphi \cos \kappa + U \cos \varphi)^2} \right) \quad (6)$$

Readers interested in the derivation of the above formulas can refer to (Morgan, 2004). So far, the relationships between the non-linear and linear forms of the parallel projection model are established. It is important to remember that the linear model is preferred in cases where GCP are available, while the non-linear model is preferred if scanner navigation data are available. Section 4 deals with the latter case. But first, a pre-requisite transformation prior to handling the scenes according to the parallel projection model is discussed in the next subsection.

3.4 Perspective To Parallel (PTP) Transformation

Original scenes captured by linear array scanners comply with the rigorous perspective geometry along the scan lines. Therefore, before dealing with the parallel projection model, Perspective To Parallel (PTP) transformation of the scene coordinates are required. Such a transformation alters the scene coordinates along the scan lines in such a way to make them comply with parallel projection (Ono et al., 1999). The mathematical model for this transformation requires the knowledge of the scanner roll angle, ψ , and is expressed as:

$$y' = y \frac{1}{1 - \frac{y}{c} \tan(\psi)} \quad (7)$$

where:

c is the scanner principal distance; and
 y', y are the coordinates along the scan line according to parallel and perspective geometry, respectively.

Therefore, any coordinate along the scanning direction can be transformed from its perspective geometry, y , to another coordinate according to parallel projection, y' . One has to note that the mathematical model in Equation 7 assumes a flat terrain. Morgan (2004) used GCP for estimating the scanner roll angle together with the parameters associated with the parallel projection. This model is expressed as:

$$\begin{aligned} x &= A_1 X + A_2 Y + A_3 Z + A_4 \\ y &= \frac{A_5 X + A_6 Y + A_7 Z + A_8}{1 + \frac{\tan(\psi)}{c} (A_5 X + A_6 Y + A_7 Z + A_8)} \end{aligned} \quad (8)$$

In the above model, measured coordinates from the scenes (x, y) are used directly to estimate the 2-D Affine parameters together with the scanner roll angle. The next section deals with an alternative approach for obtaining the scene parallel projection parameters – that is when scanner navigation data are available.

4. THE RELATIONSHIP BETWEEN THE NAVIGATION DATA AND PARALLEL PROJECTION PARAMETERS

Referring to the discussion in Section 3.1, space scanners can be assumed to travel with constant attitude ($\omega_s, \varphi_s, \kappa_s$) and constant velocity $V_s(\Delta X, \Delta Y, \Delta Z)$ during the scene capture, starting from

(X_0, Y_0, Z_0) as the exposure station of the first image. The parallel projection vector can be computed as:

$$[L \quad M \quad N] = [r_{s13} \quad r_{s23} \quad r_{s33}] \quad (9)$$

where r_{s11} to r_{s33} are the elements of the scanner rotation matrix. The scene rotation matrix R in Equations 1, may differ from the scanner rotation matrix and it can be computed as:

$$R = [\mathbf{x} \quad \mathbf{y} \quad \mathbf{z}] \quad (10)$$

where \mathbf{x} , \mathbf{y} and \mathbf{z} are unit vectors along the scene coordinate axes with respect to the object coordinate system. They can be computed as follows:

$$\begin{aligned} \mathbf{y}^T &= [r_{s12} \quad r_{s22} \quad r_{s32}] \\ \mathbf{z} &= \frac{V_s \times \mathbf{y}}{|V_s \times \mathbf{y}|} \\ \mathbf{x} &= \mathbf{y} \times \mathbf{z} \end{aligned} \quad (11)$$

The scale value of the scene can be computed as:

$$s = r_{s33} \frac{c}{Z_{0s} - Z_{av}} \quad (12)$$

where:

(X_{0s}, Y_{0s}, Z_{0s}) are the components of the exposure station at the middle of the scene;

Z_{av} is the average elevation value; and

c is the scanner principal distance.

Finally the two scene shifts can be computed as:

$$\begin{aligned} \Delta x &= s(r_{13}U - r_{11})X_{0s} + s(r_{23}U - r_{21})Y_{0s} + s(r_{33}U - r_{31})Z_{0s} \\ \Delta y &= s(r_{13}V - r_{12})X_{0s} + s(r_{23}V - r_{22})Y_{0s} + s(r_{33}V - r_{32})Z_{0s} \end{aligned} \quad (13)$$

where U and V can be computed from Equations 3. Derivation of this transformation is not listed in this paper due to its complexity. Interested reader can refer to (Morgan, 2004) for detailed derivation. So far, the derivation of scene parallel projection parameters, Equation 1, using the scanner navigation data is established. The next section deals with experimental results to verify the derived mathematical models and transformations using synthetic data.

5. EXPERIMENTS

Synthetic data are generated and tested to achieve the following objectives:

- Verifying the transformation from navigation data to scene parallel projection parameters (as discussed in Section 4);
- Verifying the transformation between the non-linear and linear forms of the parallel projection parameters (as discussed in Section 3.3);
- Analyzing the effect of PTP transformation, based on the true/estimated roll angles, on the achieved accuracy; and
- Comparing direct and indirect estimation of the parallel projection parameters.

Object space points are simulated and back-projected into stereopair using the rigorous perspective projection model. Scanner IOP are simulated similar to those of IKONOS (e.g., $c=10\text{m}$). EOP are simulated to have almost 100% stereo coverage by changing the scanner pitch angles along the flying direction, Table 1. It is assumed that the scanner's trajectory and orientation comply with the constant-velocity-constant-attitude EOP model.

Scene	X_0 Km	Y_0 Km	Z_0 Km	ΔX Km/s	ΔY Km/s	ΔZ Km/s	Roll ψ°	Pitch $^\circ$	Azimuth $^\circ$
Left	-288	60	680	7	0	0	-5	-22.5	0
Right	277	-60	680	7	0	0	5	22.5	0

Table 1. EOP used for the simulation

Twenty object space points covering an area of 11km by 11km are simulated with an average elevation of zero and a height variation of $\pm 1000\text{m}$. Figure 3 shows the distribution of the object points and the footprint of the left and right scenes. Among the object points, sixteen points are used as GCP shown as red triangles, while nine points are used as check points shown as green circles.

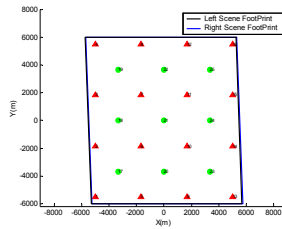


Figure 3. Object space points together with scene footprints

Using scene EOP in addition to IOP and average elevation, scene parallel projection parameters are derived, as explained in Section 4 (see Table 2).

Scene	L	M	ω°	φ°	κ°	$\Delta x, \text{m}$	$\Delta y, \text{m}$	s
Left	-3.83e-1	8.05e-2	-5	0	0	3.26e-4	0	1.35e-5
Right	3.83e-1	-8.05e-2	5	0	0	-3.26e-4	0	1.35e-5

Table 2. Derived scene parallel projection parameters

Using the derived scene parallel projection parameters, 2-D Affine parameters are derived, as explained in Section 3.3.1 (see Table 3).

Scene	A_1	A_2	A_3	A_4	A_5	A_6	A_7	A_8
Left	1.35e-5	4.89e-7	5.59e-6	3.26e-4	0	1.35e-5	-1.18e-6	0
Right	1.35e-5	4.89e-7	-5.59e-6	-3.26e-4	0	1.35e-5	1.18e-6	0

Table 3. Derived 2-D Affine parameters

Some attention must be given to the quality of the derived 2-D Affine parameters as well as PTP transformation. Space intersection is chosen as a means of examining their quality in the object space. In this case, the 2-D Affine parameters for both left and right scenes, along with left and right scene coordinates, are used. Therefore, for each scene point, two sets of 2-D Affine equations are written. For each pair of tie points, four equations can be written containing 3 unknowns, the object coordinates of the point. Thus, the object coordinates can be solved for, in a least-squares adjustment. The errors can then be computed in the object space between the estimated coordinates and the original coordinates used in the simulation. The mean and standard deviation of the errors are computed, as shown in

Table 4. These values are computed based on the total twenty-five points shown in Figure 3.

PTP transformation is also tested, based on the available scanner roll angle. The effect of performing a PTP transformation in terms of reduction of the Z-component of the errors can be seen. It can then be concluded that omitting such a correction results in large errors in the derived height values.

	Mean $_{YY} \pm \text{Std}_{YY, \text{m}}$	Mean $_Z \pm \text{Std}_Z, \text{m}$
No PTP	0.582 \pm 3.427	0.944 \pm 0.853
PTP	0.590 \pm 3.466	0.023 \pm 0.194

Table 4. Mean error and standard deviation values of the directly estimated object space points with and without Perspective-To-Parallel (PTP) correction

For the same synthetic data, the 2-D Affine parameters are indirectly estimated using GCP. Three sets of results were obtained: without PTP correction; with PTP correction using the available roll angle (the true roll angle); and with PTP correction using the estimated roll angle (Equations 8). The estimated 2-D Affine parameters and the estimated roll angles are listed in Table 5. Among the 25 object points, 16 points (seen as red triangles in Figure 3) are used as GCP in the parameter estimation. The other nine points, shown as green circles, are used as check points.

	Left scene			Right scene		
	No PTP	PTP _{true} ψ	PTP _{estimated} ψ	No PTP	PTP _{true} ψ	PTP _{estimated} ψ
$\hat{\sigma}_0$, pixels	3.47	2.61	2.60	3.95	2.63	2.58
ψ°	0.00	-5.00	-4.63	0.00	5.00	6.09
A_1	1.35e-5	1.35e-5	1.35e-5	1.35e-5	1.35e-5	1.35e-5
A_2	4.88e-7	4.88e-7	4.88e-7	4.88e-7	4.88e-7	4.88e-7
A_3	5.58e-6	5.58e-6	5.58e-6	-5.58e-6	-5.58e-6	-5.58e-6
A_4	3.26e-4	3.26e-4	3.26e-4	-3.26e-4	-3.26e-4	-3.26e-4
A_5	4.95e-9	4.81e-9	4.82e-9	4.54e-9	4.81e-9	4.87e-9
A_6	1.35e-5	1.35e-5	1.35e-5	1.35e-5	1.35e-5	1.35e-5
A_7	-1.20e-6	-1.19e-6	-1.19e-6	1.18e-6	1.17e-6	1.17e-6
A_8	1.62e-5	-7.80e-6	-6.03e-6	-3.50e-5	-1.13e-5	-6.06e-6

Table 5. Indirectly estimated 2-D Affine parameters and roll angles using GCP

As seen in Table 5, the square root of the estimated variance component, $\hat{\sigma}_0$, is the smallest by using the estimated roll angles for PTP correction. On the other hand, omitting PTP correction results in the largest estimated variance component. In addition, the estimated roll angles (as indicated in Equation 8) differ from the true roll angles. The difference is attributed to the assumption made in Section 3.4 of a flat terrain. On the other hand, it can be seen that using the estimated roll angles gives better results, in terms of the smallest variance component. In order to evaluate the quality of the estimated 2-D Affine parameters, a space intersection is performed based on the estimated parameters and the coordinates of the points in both left and right scenes, as explained earlier. The estimated object coordinates are then compared to the true values and the errors associated with the points in Tables 6.

		Mean _{xy} ±Std _{xy} ,m	Mean _z ±Std _z ,m
GCP	No PTP	0.000 ± 1.675	0.000 ± 0.858
	PTP_true ψ	0.000 ± 1.699	0.000 ± 0.070
	PTP_estimated ψ	0.000 ± 1.685	0.000 ± 0.015
Check points	No PTP	0.674 ± 1.666	0.472 ± 0.486
	PTP_true ψ	0.683 ± 1.720	0.030 ± 0.039
	PTP_estimated ψ	0.552 ± 1.690	0.002 ± 0.008

Table 6. Mean error and standard deviation of the indirectly estimated object space GCP and check points

As shown in Table 6, no bias can be seen in the estimation of object coordinates of the GCP. Again, a smaller Std_z is achieved by using the indirectly estimated roll angle, compared to those using the true roll angles. The same conclusions can be drawn for the check points (see Table 6) except for the existence of bias values. A comparison of Tables 6 and 4 reveals the suitability of indirect methods (that is, using GCP) compared to the direct methods (that is, using navigation data).

6. CONCLUSIONS AND RECOMMENDATIONS

In this paper, parallel projection is chosen to model space scenes such as IKONOS. The rationale behind selecting this model is that many space scenes have narrow AFOV and acquired in very short time. Because the original scenes comply with the rigorous perspective geometry, scene coordinates have to be altered in PTP transformation so that they comply with parallel projection. The parallel projection model is discussed together with its linear and non-linear forms and the transformation between them. The former is preferred when GCP are available while the latter is preferred when navigation data are available. The derivation of the parallel projection parameters from the navigation data is also presented. Finally, focussing on PTP transformation, a mathematical model is developed to estimate the scanner roll angles together with the scene parameters using GCP. The developed transformation and mathematical models are verified using synthetic data. Although the estimated roll angles differ from the true ones, the errors in the object space using the estimated angles are smaller. In addition, indirect parameters estimation using GCP gives smaller error values in the object space, compared to those derived using the navigation data.

Future work will include experiments using real data such as IKONOS and SPOT scenes. Inclusion of higher order primitives (such as linear and areal features) and object space constraints to the parallel projection model will be analyzed. Finally, normalized scenes, DEM and ortho-photos will be generated based on the parallel projection.

REFERENCES

Abdel-Aziz, Y., and H. Karara, 1971. Direct Linear Transformation from Comparator Coordinates into Object Space Coordinates in Close-Range Photogrammetry, *Proceedings of ASP/UI Symposium on Close Range Photogrammetry*, University of Illinois at Urbana Champaign, Urbana, Illinois, pp. 1-18.

Dowman, I., and J. Dolloff, 2000. An Evaluation of Rational Functions for Photogrammetric Restitutions, *International Archives of Photogrammetry and Remote Sensing*, 33 (Part B3): 254-266.

Ethridge, M., 1977. *Geometric Analysis of Single and Multiply Scanned Aircraft Digital Data Array*, PhD Thesis, Purdue University, West Lafayette, Indiana, 301p.

Fraser, C., H. Hanley, and T. Yamakawa, 2001. Sub-Metre Geopositioning with IKONOS GEO Imagery, *ISPRS Joint Workshop on High Resolution Mapping from Space*, Hanover, Germany, 2001.

Fritz, L., 1995. Recent Developments for Optical Earth Observation in the United States, *Photogrammetric Week*, pp75-84, Stuttgart, 1995.

Habib, A., and B. Beshah, 1998. Multi Sensor Aerial Triangulation. *ISPRS Commission III Symposium*, Columbus, Ohio, 6 – 10 July, 1998.

Habib, A., Y. Lee, and M. Morgan, 2001. Bundle Adjustment with Self-Calibration of Line Cameras using Straight Lines. *Joint Workshop of ISPRS WG I/2, I/5 and IV/7: High Resolution Mapping from Space 2001*, University of Hanover, 19-21 September, 2001.

Lee, Y., and A. Habib, 2002. Pose Estimation of Line Cameras Using Linear Features, *ISPRS Symposium of PCV'02 Photogrammetric Computer Vision*, Graz, Austria.

Lee, C., H. Theiss, J. Bethel, and E. Mikhail, 2000. Rigorous Mathematical Modeling of Airborne Pushbroom Imaging Systems, *Journal of Photogrammetric Engineering & Remote Sensing*, 66(4): 385-392.

McGlone, C., and E. Mikhail, 1981. Photogrammetric Analysis of Aircraft Multispectral Scanner Data, *School of Civil Engineering, Purdue University*, West Lafayette, Indiana, 178p.

Morgan, M., 2004. *Epipolar Resampling of Linear Array Scanner Scenes*, PhD Dissertation, Department of Geomatics Engineering, University of Calgary, Canada.

Ono, T., Y. Honmachi, and S. Ku, 1999. Epipolar Resampling of High Resolution Satellite Imagery, *Joint Workshop of ISPRS WG I/1, I/3 and IV/4 Sensors and Mapping from Space*.

Tao, V. and Y. Hu, 2001. A Comprehensive Study for Rational Function Model for Photogrammetric Processing, *Journal of Photogrammetric Engineering & Remote Sensing*, 67(12):1347-1357.

Wang, Y., 1999. Automated Triangulation of Linear Scanner Imagery, *Joint Workshop of ISPRS WG I/1, I/3 and IV/4 on Sensors and Mapping from Space*, Hanover, 1999.